Nonlinear Propagation of a Randomized Laser Beam through an Expanding Plasma

J. Myatt,[1,2] D. Pesme,[2] S. Hüller,[2] A. Maximov,[1] W. Rozmus,[1] and C. E. Capjack[3]

[1]*Theoretical Physics Institute, Department of Physics, University of Alberta, Edmonton, Alberta, Canada T6G 2J1*

[2]*Centre de Physique Théorique, Ecole Polytechnique, 91128 Palaiseau Cedex, France*

[3]*Department of Electrical Engineering, University of Alberta, Edmonton, Alberta, Canada T6G 2G7*

(Received 18 July 2001; published 30 November 2001)

We present simulations of the interaction of a random phase plate laser beam with an underdense, expanding plasma for conditions typical of recent LULI experiments. We use a new code that describes the paraxial propagation of the laser, accounting for the nonlinear evolution of the plasma in an isothermal fluid description with weakly collisional electrons. The transmitted light, in excellent agreement with experiment, is shown to be strongly redshifted as a result of self-phase modulation due to self-focusing.

DOI: 10.1103/PhysRevLett.87.255003 PACS numbers: 52.38.Hb, 52.20.Fs, 52.35.Mw, 52.38.Bv

An understanding of the nonlinear propagation of intense laser beams through underdense plasma is a basic problem of outstanding theoretical interest [1,2]. It is also an important issue for both laser fusion and other applications such as x-ray sources and laser particle accelerators that require the propagation of laser light through large regions of underdense plasma. Recently, plasma-induced laser beam incoherence (LBI) generated by the nonlinear interaction of intense laser light, with and without random phase plates (RPP), with underdense plasma has been observed in simulations [3,4] and experiment [5–7]. Random phase plates produce a regular speckle intensity distribution, rather than the otherwise irregular pattern that would be a result of the aberrations always present in large glass lasers. Theoretical work has shown that LBI can arise as a result of forward scattering processes such as nonstationary filamentation, stimulated Brillouin scattering (SBS) [2,3], and more recently, the resonant instability of filaments [8]. Despite this, the connection with experiment is at present rather poor. Experimental signatures of LBI include increased temporal bandwidth and angular divergence of the beam. Uncontrolled beam spray (spatial LBI) is unwanted and can lead to poor symmetry and target coupling. On the other hand, increased temporal incoherence has been shown to reduce the levels of laser driven parametric instabilities that are detrimental to successful fusion schemes [9,10]. This observation has led to the implementation of external smoothing schemes generating spatial and/or temporal incoherence on all large lasers [10]. A better physical understanding of plasma-induced LBI might make the expensive, externally generated bandwidth redundant.

In this Letter, we provide an explanation for recent experiments conducted at the "Laboratoire pour l'Utilisation des Lasers Intenses" (LULI) facility in France. These well-diagnosed and well-characterized experiments set out to investigate plasma-induced LBI in a regime of high plasma density $n_e/n_c \sim 0.2$–0.7, which are complementary to previous experiments carried out at lower density $n_e/n_c \sim 0.07$ [5,6]. Here, $n_c = m_e\omega_0^2/4\pi e^2$ is the critical electron density and ω_0 is the laser frequency. The higher density is more relevant for direct drive fusion where light illuminates the target directly and propagates to the critical surface. The transmitted light spectra and angular distribution were strikingly different from previous results [5,6] and lack a convincing explanation as to their origin.

Experimental evidence for plasma-induced LBI.— Channel formation due to self-focusing and beam spray at angles consistent with the fastest growing mode of the filamentation instability were first reported in underdense exploding foil plasmas [5]. Later Nova experiments at $n_e/n_c = 0.07$ investigated the angular divergence and spectral composition of the transmitted light [6]. Here, scattering angles well outside the laser cone were observed, and the initially coherent light was broadened and redshifted in frequency. Because of the measured size and angular dependence of the redshift $\delta\omega = \omega_0 - \omega$ in the scattered light the active mechanism was identified as forward stimulated Brillouin scattering (fSBS). In SBS incident light is scattered by ion acoustic waves (IAW), giving a scattered electromagnetic (EM) wave that is lower in frequency by the IAW frequency, $\delta\omega = \omega_s = k_s c_s$, where $c_s = \sqrt{(ZT_e + 3T_i)/M_i}$ is the IAW sound speed, T_e and T_i are the electron and ion temperatures, M_i is the ion mass, and Z is the ion charge. This frequency is proportional to the magnitude of the IAW wave number k_s, which depends on the scattering angle θ, according to $k_s = 2k_{00}\sqrt{1 - n_e/n_c}\sin(\theta/2)$, where $k_{00} = \omega_0/c$ is the vacuum wave number (in the stimulated process, the beating of the EM waves reinforce the sound wave, leading to exponential growth).

The more recent LULI experimental results of laser-plasma coupling at higher plasma density $n_e/n_c \sim 0.2$–0.7 and high intensity have shown different behavior. Beyond a threshold intensity, much larger frequency shifts in the transmitted light spectrum were seen [7]. Figures 1a and 1b, taken from Ref. [7], show the experimental frequency spectrum of transmitted light falling in the aperture $\theta = 0° \pm 10°$ for the case of a 1 μm wavelength, $\lambda_0 = 1.053$ μm, interaction beam with $f/6$ RPP optics, $(n_e/n_c)_{\max} = 0.4$, $T_e = 600$ eV, and CH (Parylene) targets with $Z_{\text{eff}} \equiv \langle Z^2\rangle/\langle Z\rangle = 5.3$.

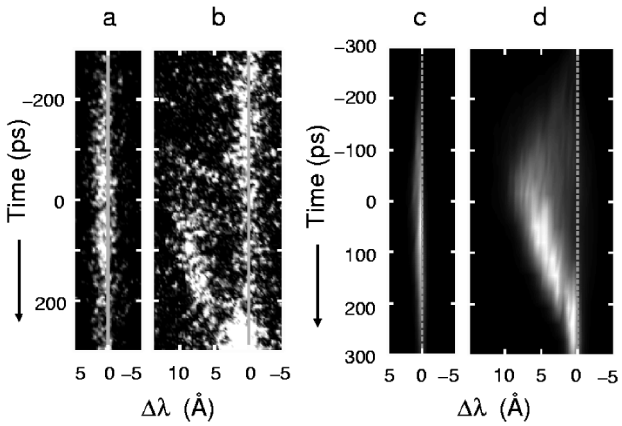

FIG. 1. Experimental transmitted light spectra, collected over angles $0° \pm 10°$ from forward, taken from Ref. [7] (a) and (b), and the corresponding spectra from simulations (c) and (d). Parameters are as in text, and laser intensities are $\langle I \rangle_{14} = 0.1, 0.45$ in (a),(c) and (b),(d), respectively.

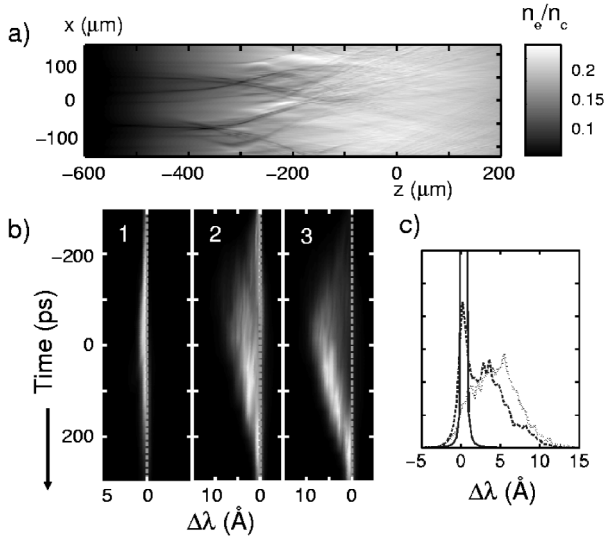

FIG. 2. Simulation results for the same parameters as Figs. 1(b),(d): Plot (a) shows the plasma density at $t = 0$. The 1 μm thick target was positioned at $z = 0$, and its expansion is evident. The laser is incident from the left. Plot (b) shows the frequency spectra of forward-going light as a function of time taken at the axial locations $z = -400$ μm (1), $z = -180$ μm (2), and $z = 200$ μm (3). Plot (c) is a lineout of (b) taken at $t = -100$ ps.

The average laser intensity in Figs. 1a and 1b, $\langle I \rangle = 0.1$, and 0.45×10^{14} W/cm^2, respectively. Light was also collected in the aperture $22.5° \pm 5°$, and although not shown, had similar spectral characteristics. In Fig. 1b two distinct components of the transmitted light spectra are seen, a narrow unshifted feature and a broad satellite that is redshifted by up to $\Delta\lambda = \lambda_s - \lambda_0 \sim 10$ Å, where the corresponding frequency shift is $\delta\omega(\mathrm{ps}^{-1}) = [0.188/\lambda_0^2(\mu\mathrm{m})]\Delta\lambda(\text{Å})$. An interpretation of the redshifted wing in terms of fSBS runs into serious difficulties: the shift should scale linearly with scattering angle; instead it is insensitive. Furthermore, a 10 Å shift in wavelength corresponds to a frequency $\delta\omega/k_{00}c_s \sim 2$, which is 30 times larger than fSBS can produce in this angle: $\omega_s/k_{00}c_s = 2\sqrt{1 - n_e/n_c}\sin(10°/2) \sim 0.07$. An explanation of the LBI for this experiment requires a new mechanism and challenges our basic understanding of the process. In an attempt to resolve this issue we have made detailed numerical simulations using a new laser plasma interaction (LPI) code.

Numerical simulations of high density experiments.— Our code HARMONHY models the plasma as a nonlinear fluid and propagates the light using the paraxial approximation with an approach similar to that used by the LPI code F3D [11]. The simulations presented here have been made as realistic as possible and include the interplay between strong inverse bremsstrahlung (IB) absorption, laser pulse temporal profile, and target expansion. The inclusion of these effects has previously been shown to be essential in modeling the spatiotemporal behavior of parametric instabilities in these experiments [12]. Here, backward SBS and stimulated Raman scattering (SRS) are not modeled as they are not energetically important in this context; experimental reflectivites are on, or below, the percent level. The numerical simulations model a two-dimensional plasma slab, shown in Fig. 2a, of dimensions sufficiently large to be comparable with the focal spot of the interaction beam [7]. The $f/6$ random phase plate optics used in the experiment are modeled with the standard "top-hat" prescription that, in vacuum, would produce a speckle pattern of characteristic axial dimensions $l_{||} \sim 8f^2\lambda_0$, transverse dimension $l_\perp \sim f\lambda_0$, and intensity distribution with known statistical properties [13]. The average laser intensity has a Gaussian profile in time having its peak intensity at $t = 0$ with a 600 ps FWHM. The principal axis of the plasma expansion is coincident with the laser propagation direction and defines the z axis. The simulation region is taken to be 800 μm in the axial (z) direction, which is larger than both the density scale length $L_n \sim (450\text{–}600)$ μm, and velocity scale length $L_v \sim (100\text{–}120)$ μm. The box is 240 μm in transverse extent, and periodic. The plasma is globally isothermal to be consistent with experimental Thomson scattering measurements [14], with an electron temperature of $T_e = 600$ eV. Electron collisions play an important role in self-focusing since, due to the low electron temperature, the electron-ion collisional mean-free path, $l_{ei} = 13.2T_e^2(\mathrm{keV})\lambda_0^2(\mu\mathrm{m})/[Z_{\mathrm{eff}}(n_e/n_c)\,(\Lambda/10)] \sim 3$ μm is of the same order as the transverse speckle size $l_\perp \sim 6$ μm (for $n_e/n_c = 0.4$). Because of this we have implemented the nonlocal electron transport model of Ref. [15] that effectively results in an augmentation of the ponderomotive force due to finite heating effects. This effectively lowers the threshold intensity for self-focusing, but the resulting behavior is essentially the same as in the

ponderomotive case at laser intensities a few times higher [16]. Without this contribution, the simulations show very little self-focusing which is in clear contradiction with experiment.

Target expansion is self-consistently reproduced in the simulations and produces similar density and velocity profiles to those that have been experimentally determined via Thomson scattering measurements [14]. The peak density $n_{\max} = \max\{n_e\}$ falls in an exponential fashion $n_{\max}(t) \sim n_{\max}(0)\exp(-t/t_c)$ with a time constant of $\sim$500 ps comparable to the duration of the interaction pulse. Hence the plasma becomes significantly more transparent at later times. For CH (Parylene) targets the IB absorption length $L_{\mathrm{IB}} = [(n_e/n_c)\nu_{ei}/V_g]^{-1}$ is 160 and 740 μm for $n_e/n_c = 0.4$ and $n_e/n_c = 0.2$, respectively. The transmission increases from $\sim$2% at $t = -200$ ps to 35% at peak laser intensity, in good agreement with experimental observations [7]. As far as we are aware, these are the first large-scale, multidimensional simulations of the LULI plasma to date that include the dynamics of the target expansion into the vacuum, simulate the entire duration of the interaction beam, and at the same time describe the microscopic behavior of fSBS and self-focusing.

Simulation results.—Results corresponding to the experiments of [7,14] with $(n_e/n_c)_{\max} = 0.4$, and $\langle I\rangle_{14} = 0.45$ are shown in Figs. 1d and 2. The simulated experiment proceeds as follows: the interaction beam propagates up the density profile, leading to the emergence of channels in the plasma density at the locations of intense speckles in the RPP far field, as a result of the ponderomotive and thermal pressure of the light (Fig. 2a). At some point in the density profile these become unstable to the self-focusing instability and start to contract transversally. The condition for self-focusing instability is that the power p contained within a laser speckle should exceed some critical value $p/p_c \equiv P > 1$. For pure ponderomotive pressure in 2D $P_{2\mathrm{D}} \sim 0.42\langle v_{osc}^2\rangle/v_{Th}^2 f^2 n_e/n_c > 1$, where $\langle v_{osc}^2\rangle/v_{Th}^2 \sim 0.03(\lambda_0/1\ \mu\mathrm{m})^2(I/10^{14}\ \mathrm{W/cm^2})(600\ \mathrm{eV}/T_e)$ [4]. Taking for example a speckle of intensity $I = 6\langle I\rangle$ this condition $P_{2\mathrm{D}} \gg 1$ can be satisfied only for densities $n_e/n_c > 0.2$. This is hard to achieve as the regions of high intensity and high density have little overlap due to IB absorption. This shows the importance of the thermal contribution that effectively decreases the critical power, p_c [16]. The contraction is saturated by density depletion, which is observed to be anywhere up to 80%. Channel formation and evolution displays a complicated temporal behavior, which is evident in Fig. 2a. Interestingly, we find that formation of a quasistatic channel develops, not on the short transient time scale usually estimated by the acoustic transit time $a_0/c_s \sim 20$ ps across a speckle radius $a_0 \sim f\lambda_0$, but continuously evolves entrained to the long time variation of the laser pulse. The channels are seen to terminate as a result of instability of the "equilibrium" filament just before the density maximum ($z = -200$ μm in Fig. 2a). This is evident in Fig. 2a. On the back side of the target ($z > 0$), there is a broad spectrum of ion waves, that by a spectral analysis, have been shown to be transversely propagating ion waves associated with stimulated forward scattering of the light. The density perturbation level here is much lower that on the front side ($z < 0$).

Explanation of the strong redshift.—The experimental and simulated transmitted light spectra are in excellent agreement, as can be seen in Fig. 1. Both display a time dependent redshift $\Delta\lambda$ that reaches $\Delta\lambda \sim 10$ Å at peak laser intensity. We can explain the transmitted light spectra, Figs. 1a and 1b, by thinking in terms of an ensemble of RPP speckles. Figure 3a shows a small part of the simulation box containing an isolated filament that has formed from a laser speckle of $I \sim 6\langle I\rangle$, late in the strongly nonlinear stage of its evolution. On route to this state, first the channel elongated and then developed strong longitudinal modulations characteristic of the "sausage" or "necking" instability [17]. This can still be identified in the portion of the channel $0 < z < 100$ μm in Fig. 3a. Radiation emission from the channel is also evident in this same region $0 < z < 100$ μm [18]. The density holes, corresponding to intensity maxima along the channel, deepen and the channel lengthens rapidly with rising laser intensity. This effect gives rise to a red frequency shift, as a result of the increased index of refraction in the channel.

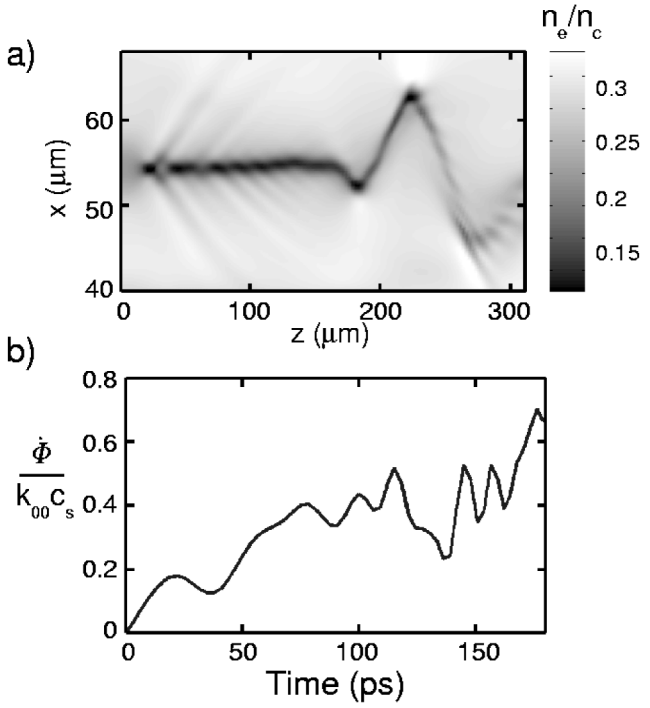

FIG. 3. Plot (a) shows a small region of the total simulation volume taken at peak laser intensity that contains a single self-focused laser speckle. Plot (b) shows an estimate of the time dependent phase shift of the trapped light using Eq. (1).

This frequency shift $\delta\omega$ has been estimated by taking a one-dimensional slice of the density $\delta n_{1D}(z,t)$ along the axis of the filament and calculating the time derivative of the resulting shift in phase Φ [8]:

$$\delta\omega(z,t) = -\frac{\partial}{\partial t}\Phi(z,t) = \frac{k_0}{2n_c}\frac{\partial}{\partial t}\int_0^z \delta n_{1D}(z',t)\,dz'. \quad (1)$$

This estimate is shown in Fig. 3b and approaches $\delta\omega = 0.8k_{00}c_s$ for the particular speckle shown. Hot spots containing less trapped power generate smaller density depressions, and a smaller frequency shift. At later times, shown in Fig. 3a, curvature develops in the channel which increases to bend in time until the radiation breaks through the walls of the snaking density channel, exciting a broad spectrum of ion waves, which provide both a density and electromagnetic seed for fSBS. This hosing instability [19] provides a further redshift (not shown in Fig. 3b) due to the increased path length in the curving channel.

Figure 2b shows the spatial dependence of the frequency spectrum of forward propagating light obtained by taking transverse slices of the electric field amplitude E at various axial locations. Panel 1 in Fig. 2b corresponds to an axial location where the density channels have not yet self-focused. There is a small frequency shift $\sim$0.7 Å due to a slight ponderomotive evacuation of density from the hot spot. Panel 2 of this figure corresponds to $z = -180$ μm. This is the point where filaments first become unstable and break up. This spectrum is a combination of shifted light that was trapped inside self-focused filaments, and light that was not trapped and remains unshifted. Importantly, the light has obtained almost all of its spectral width $\sim$7 Å at this point due to self-phase modulation and filament instability. Panel 3 shows the light at the exit plane of the simulation which has undergone some further shifting during its propagation from $z = -180$ μm to $z = 200$ μm, resulting in a final shift of up to 9 Å. This is made obvious in Fig. 2c, which shows a lineout of the spectra. Spectral diagnostics show that in the region $-200 < z < 200$ μm there is significant stimulated forward scattering of both the shifted and unshifted components from transverse ion waves. This has been seeded by the filament instability that provides both an electromagnetic and ion-wave seed. The angular divergence of the beam is quite large at this point $\sim \pm 30°$ and is consistent with experimental observations.

We claim complete success in understanding the experimental spectra. The difference in contrast between early and late times, reproduced in the simulations, is a result of the effect of plasma expansion on IB absorption. The threshold for the redshift occurs at the experimentally observed intensity between $\langle I\rangle_{14} = (0.1-0.45)$ as a result of electron collisions. Furthermore, for the higher intensity and at peak laser intensity both experimental and simulation spectra show a broad redshift of similar magnitude that is a result of self-phase modulation of light trapped in self-focused filaments and filament instability, further enhanced by classical fSBS. The rate of channel digging slows at later times and fSBS overtakes self-phase modulation as the dominant effect.

Conclusions.—Good agreement is found with experimental spectra only if the electron collisional augmentation of the ponderomotive force is taken into account. Significantly, this gives a strong demonstration of the insufficiency of ponderomotive self-focusing in explaining the results of LULI experiments. The mechanism for producing the LBI is predominantly self-phase modulation and filament instability, followed by fSBS, in contrast to experiments at lower density [6], where the smaller redshift in the transmitted light spectra were consistent with forward SBS alone. At lower density the density depressions are not as deep, nor as effective at self-modulation, and the contribution due to the fSBS is dominant; at high density the opposite is true. These results obtained here can be used to examine problems associated with models of backward SBS and SRS in these plasmas that ignore the important plasma-induced LBI effect [12].

We thank J. Fuchs and C. Labaune for useful discussion. This work was supported by the Natural Sciences and Engineering Research Council of Canada. J. M. was partially funded by the Marie Curie fellowship within the framework of the European Communities Training and Mobility of Researchers (TMR) program. The numerical simulations were performed at the "Institut du Développement et des Ressources en Informatique Scientifique (IDRIS) facility in France.

[1] C. H. Still *et al.,* Phys. Plasmas **7**, 2023 (2000).
[2] V. V. Elisseev *et al.,* Phys. Plasmas **4**, 4333 (1997).
[3] A. J. Schmitt *et al.,* Phys. Plasmas **5**, 503 (1998).
[4] A. Maximov *et al.,* Phys. Plasmas **8**, 1319 (2001).
[5] P. Young *et al.,* Phys. Plasmas **2**, 2825 (1995).
[6] J. D. Moody *et al.,* Phys. Rev. Lett. **83**, 1783 (1999).
[7] J. Fuchs *et al.,* Phys. Rev. Lett. **86**, 432 (2001).
[8] D. Pesme *et al.,* Phys. Rev. Lett. **84**, 278 (2000).
[9] J. D. Moody *et al.,* Phys. Rev. Lett. **86**, 2810 (2001).
[10] J. Lindl, Phys. Plasmas **2**, 3933 (1995).
[11] R. Berger *et al.,* Phys. Plasmas **5**, 4337 (1998).
[12] V. T. Tikhonchuk *et al.,* Phys. Plasmas **8**, 1636 (2001).
[13] H. Rose, Phys. Plasmas **3**, 1709 (1996).
[14] J. Fuchs *et al.,* Phys. Plasmas **7**, 4659 (2000).
[15] A. V. Brantov *et al.,* Phys. Plasmas **5**, 2742 (1998).
[16] V. Yu. Bychenkov *et al.,* Phys. Plasmas **7**, 441 (2000); **7**, 1511 (2000).
[17] E. J. Valeo *et al.,* Phys. Rev. Lett. **34**, 1008 (1975).
[18] F. Vidal *et al.,* Phys. Rev. E **55**, 3571 (1997).
[19] E. Valeo, Phys. Fluids **17**, 1391 (1974).